NANO LETTERS

2008
Vol. 8, No. 5
1374-1381

Ultrafast Exciton Fine Structure Relaxation Dynamics in Lead Chalcogenide Nanocrystals

Justin C. Johnson,* Kathrine A. Gerth, Qing Song, James E. Murphy, and Arthur J. Nozik*

National Renewable Energy Laboratory, 1617 Cole Boulevard, Golden, Colorado 80401

Gregory D. Scholes

Department of Chemistry, 80 St. George Street, Institute for Optical Sciences, and Center for Quantum Information and Quantum Control, University of Toronto,

Toronto, Ontario M5S3H6, Canada

Received January 14, 2008; Revised Manuscript Received March 4, 2008

ABSTRACT

The rates of fine structure relaxation in PbS, PbSe, and PbTe nanocrystals were measured on a femtosecond time scale as a function of temperature with no applied magnetic field by cross-polarized transient grating spectroscopy (CPTG) and circularly polarized pump–probe spectroscopy. The relaxation rates among exciton fine structure states follow trends with nanocrystal composition and size that are consistent with the expected influence of material dependent spin–orbit coupling, confinement enhanced electron–hole exchange interaction, and splitting between L valleys that are degenerate in the bulk. The size dependence of the fine structure relaxation rate is considerably different from what is observed for small CdSe nanocrystals, which appears to result from the unique material properties of the highly confined lead chalcogenide quantum dots. Modeling and qualitative considerations lead to conclusions about the fine structure of the lowest exciton absorption band, which has a potentially significant bearing on photophysical processes that make these materials attractive for practical purposes.

Introduction. Spin relaxation and dephasing dynamics of electrons in self-assembled semiconductor quantum dots (QD) have received recent attention because they are an essential component of quantum computing and "spintronics" applications.[1] In colloidal nanocrystals (NC), spin dynamics have been much less frequently studied, although in addition to applications in spintronics, studying spin states in NCs represents a route for understanding the fine structure of optical excitations in various quantum confinement regimes. Recent developments in the study of fine structure relaxation dynamics in colloidal CdSe NCs have led to a greater understanding of the role of quantum confinement in determining the fine structure of exciton states.[2–7] Unlike the recently studied CdSe NCs, lead chalcogenides have a narrow band gap, large dielectric constants, and nearly equivalent electron and hole masses.[8–11] The unique material parameters in addition to the very strong quantum confinement achievable in these NCs makes detailed fundamental studies of the nature of fine structure states in these samples highly desirable.

Lead chalcogenide NCs have also been the focus of recent studies largely due to the discovery and characterization of multiple exciton generation (MEG) in these materials.[12–14] Models of the MEG process that have been recently proposed cannot yet fully explain all experimental results, and in many ways the understanding of the effect suffers from insufficient definitive information about the nature of the exciton states that make up the absorption bands of these NCs. Although the focus of our investigation lies in measuring the transition rates among the fine structure states in the lowest exciton band only, the underlying physical interactions that give rise to these transitions may play a role in determining multiexciton effects that have an influence on MEG. For example, the strength of electron–phonon interactions in NCs that play a crucial role in fine structure relaxation dynamics also affect exciton dephasing and cooling rates, which are expected to influence the efficiency of MEG.[15]

Despite their potential practical advantages in some applications, colloidal NCs are often more difficult to

* Corresponding authors. E-mail: justin_johnson@nrel.gov (J.C.J.); arthur_nozik@nrel.gov (A.J.N.).

10.1021/nl080126a CCC: $40.75
Published on Web 04/01/2008

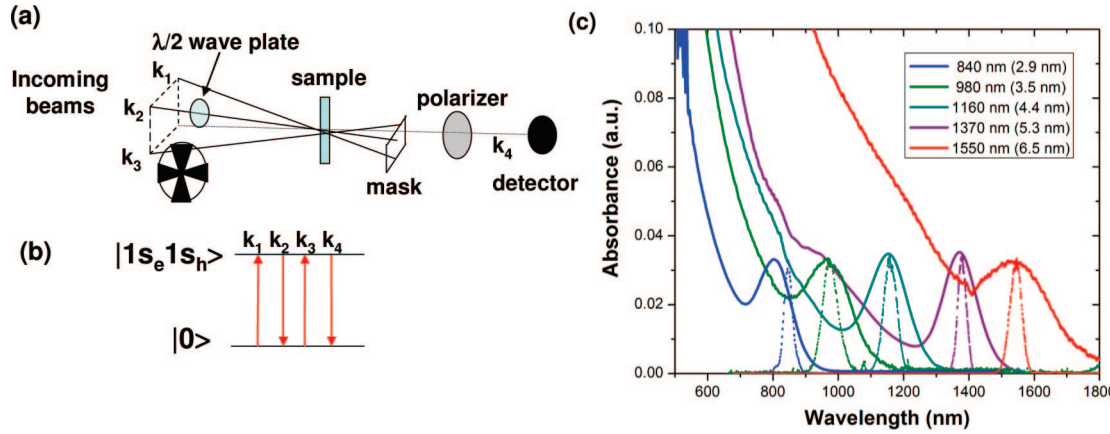

Figure 1. (a) Experimental configuration, showing beam alignment in "boxcar" phase matching arrangement. (b) Photon energy diagram illustrating the transient grating process at the first exciton absorption peak of a PbX NC. (c) Absorption (solid) and laser (dotted) spectra for selected PbS CPTG experiments.

investigate spectroscopically than self-assembled QDs due to the random orientation of the NCs in solutions or films and the large size dispersion of as-prepared samples. However, it has been demonstrated that these obstacles can be partially overcome by appropriate application of nonlinear coherent spectroscopy.[16,17] In particular, different forms of four-wave mixing (FWM) are capable of obtaining high-resolution information despite inhomogeneous broadening. Another recent development involving FWM experiments is that cross-polarized transient grating (CPTG) spectroscopy has been applied to study fine structure relaxation dynamics in randomly oriented CdSe NCs.[2–6] CPTG utilizes the coherent nature of the TG signal in order to determine the history of the angular momentum projection of a NC rather than its absolute orientation. In this manner, an effective rate of electron or hole spin-flipping can be measured on a rotationally isotropic ensemble of colloidal NCs.

Conventional transient grating spectroscopy is a form of four-wave mixing in which two pump beams crossed at an angle in a sample create a spatially modulated excited-state population. A third pulse diffracts from this population grating in the phase-matched direction, allowing for background-free determination of population dynamics. In cross-polarized transient grating experiments, no population grating is formed. If one considers the formalism for oriented crystals, an intuitive interpretation of the CPTG experiment is that a polarization grating is formed due to the fact that the polarization in the sample varies across a grating fringe from left to right circular,[18] thus exciting oppositely aligned spin states. The diffracted signal from the third beam will then decay according to the relaxation of spin orientation (or angular momentum projection), which can occur by rotational diffusion or relaxation among fine structure levels.

Figure 1b shows the photon energy diagram for the transient grating experiment. The first two pulses interact with the sample to create a population of single exciton states according to the transition dipole moments from the ground state, with each NC exciton initially having well-defined angular momentum projection. The third pulse generates a coherence which is emitted in the phase-matched direction. Because the sample is a solution of randomly oriented NCs, during the course of the experiment there is never predominantly one fine structure state with a particular angular momentum orientation versus another; the distribution of angular momentum orientation states is isotropic. However, the cross-polarized excitation still imparts angular momentum to the NCs, and for an individual NC, the phase of the third-order polarization evolves according to whether or not the angular momentum of the exciton has changed sign from its original orientation. As the nonlinear coherent signal involves contributions from each NC (including the phase), the total signal is a sensitive probe of fine structure relaxation dynamics. It is important to note that change of NC orientation by rotational diffusion occurs on a much slower time scale in our samples and does not contribute to the decay of the signal observed in CPTG.

Although the CPTG signal is a convolution of spin and population relaxation components, in well-passivated lead salt NCs, the spin relaxation is orders of magnitude faster than population decay, yielding dynamics that are not influenced by trapping, recombination, or other exciton population loss mechanisms. The CPTG dynamics can be modeled by tracking the evolution of the third-order polarization, which is derived for a specific experiment by utilizing density matrix formalism. In our case, the CPTG signal is proportional to the difference between the population of NCs with excitons that have not undergone a transition to an opposite angular momentum state and the NCs that have undergone such a transition. Considering just the bright fine structure states of the lowest exciton of a NC with wurtzite crystal structure as a simple case, a direct exciton spin-flip corresponds to a change in the projection of angular momentum from $+(-)1$ to $-(+)1$. This can be also be envisioned as a simultaneous electron and hole spin-flip, which is mediated by electron–hole exchange interactions. A change in the angular momentum orientation can also be induced by independent electron and hole spin-flips thus involving transitions between bright and dark exciton states. This mechanism is expected to be influenced by spin–orbit coupling (among other factors), which may play an increasingly important role in dictating spin-flip dynamics in strongly confined systems consisting of heavy atoms.

In several recent studies, it was determined that the fine structure relaxation rate in CdSe NCs follows a $1/r^4$ dependence on the NC radius. Assuming that Fermi's golden rule relates this relaxation rate and the energy splitting, the size dependence of the splitting in CdSe NC goes as $1/r^2$. Through additional studies on nanorods, it was further discovered that only the cross-sectional area (or simply the diameter of dots or rods) of the CdSe NC is important for determining the fine structure relaxation rate between bright and dark states. Much larger CdSe nanorods were also recently studied and found to exhibit biexponential decay kinetics, although the second decay component did not show any dependence on size. Kinetic modeling confirms the presence of two distinct decay components, including a fast hole spin-flip and another slower pathway yet to be identified.

Until very recently, definitive theoretical information about the fine structure states in the lowest exciton band of lead chalcogenide QDs has been elusive. Simple effective mass models are inaccurate for PbX because of the considerable nonparabolicity of the bands that comprise the lowest exciton states.[19] Multiband **k·p** formalism has been utilized to calculate the energy level structure; however, these calculations neglect intervalley scattering between the four equivalent bands at the L point and thus may not accurately represent the true fine structure.[20] Semiempirical pseudopotential methods, which treat the problem more comprehensively, may provide some insight. An et al.[21] have recently calculated the lowest exciton fine structure using this method. The results predict 64 possible exciton states within this band, some of which are split by intervalley scattering and exchange interaction. Not including intervalley scattering, three bright states and one dark state are predicted to exist at the bottom of the lowest exciton feature, separated from each other by the exchange splitting. These states, unlike those predicted from CdSe (with well-defined angular momentum quantum numbers[22]), have considerable admixture of both "singlet" and "triplet" character partially because of the large spin-orbit coupling in the PbX NCs that heavily intermixes pure exciton spin states. Exciton eigenstates are then best identified by their projection of total angular momentum instead of their quasiparticle spin alignment. Although employing a density matrix approach including all 64 states to model the spin-flip decay is not yet possible, the results of CPTG experiments are still interpretable based upon the principles outlined above. Indeed, an experimental study may lead to an understanding that can inform theory about the nature of states predicted to exist in the fine structure of lead chalcogenide NCs.

Experimental Section. Varying sizes of PbS NCs were purchased from Evident Technologies. Additional PbS, PbSe, and PbTe NCs were synthesized according to published procedures.[13,14,23] Various methods of characterization performed previously on samples synthesized by these methods confirms that samples used for spectroscopic experiments have narrow size distributions (~10%), long photoluminescence (PL) lifetimes (>500 ns), high PL quantum yields (~50%), and no significant fast trapping of charge carriers. The NCs, all capped in oleic acid, were suspended in hexane for all spectroscopic studies because the NCs were highly soluble and stable in this solvent and hexane produced only a small, instantaneous TG signal. Samples were carefully cleaned and filtered of all large scattering impurities before being used in experiments because a scattering background is typically the largest source of noise in the TG signal. The sample was contained in a sealed 1 mm path length glass cuvette for all room temperature optical studies. Typical optical densities at the peak of the exciton absorption were 0.05–0.2. Low temperature studies were performed by dispersing the NCs in a glass-forming solvent (heptamethylnonane (HMN)), which was then cooled by a closed-loop He cryostat.

The experimental setup is depicted in Figure 1a. A frequency-doubled 1 kHz Ti:sapphire amplified laser (Clark, CPA 2001, 775 nm fundamental) was used to pump a two-stage noncollinear optical parametric amplifier (NOPA). A small fraction of the 775 nm beam was focused into a 2 mm thick sapphire plate to provide the near-infrared seed for the NOPA. The remainder of the 775 nm was frequency doubled in a 0.4 mm BBO crystal and split 20:80 into the first and second stage NOPA pump beams. The NOPA provides tunable pulses from 840 to 1600 nm, with pulse energies varying from 1 to 5 μJ. After compression in F2 glass prisms, the pulse widths range from 25 to 30 fs (840–1050 nm), then linearly increasing from about 35 fs at 1100 nm to about 55 fs at 1600 nm. No additional advantage was gained from compressing pulses with wavelengths longer than 1500 nm; therefore, these pulses were used without compression. Pulse overlap and cross-correlations were determined by detecting sum-frequency generation in a 0.05 mm BBO crystal placed at the sample position.

The NOPA output was split into three beams of approximately equal power, and each beam was directed to a delay stage. The pulses were attenuated to <50 nJ each and aligned in a boxcar configuration, with the probe beam (k_3) chopped at 500 Hz. The beams traveled collinearly to a spherical silver mirror and were focused to a common point at an angle of approximately 3°. The probe pulse was delayed with respect to k_1 and k_2, which were overlapped temporally. The polarization of k_1 and k_3 were set to be equal for all experiments, while the polarization of k_2 could be controlled with a $\lambda/2$ wave plate. The signal was isolated in the phase-matched direction ($k_s = k_2 - k_1 + k_3$) at the fourth corner of the box and detected with an InGaAs photodiode. A polarizer was placed in front of the detector to select a specific polarization component. The 500 Hz frequency component of this signal was isolated with a lock-in amplifier. Pump–probe experiments were undertaken by blocking k_1 and detecting k_3 directly. Pump and probe beams were set to either right (R) or left (L) circular polarization with $\lambda/4$ waveplates.

Results. Figure 1c displays the absorption spectra and NOPA pulse spectra for some of the PbS NCs tested. The diameter of the PbS NCs ranged from 2.9 to 6.6 nm, which corresponds to a lowest exciton absorption band peaking from 800 to 1560 nm. Although we are able to synthesize larger NCs, their exciton absorption was outside the attain-

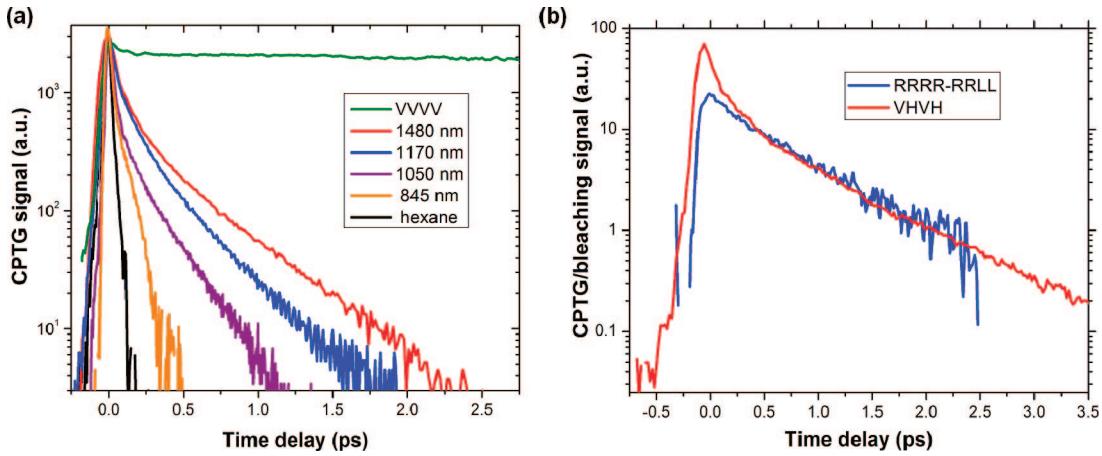

Figure 2. (a) Representative raw kinetic data for population (VVVV) and polarization grating dynamics in various PbS NC samples. The decreasing decay rate with larger NCs is evident. (b) Comparison of CPTG and circularly polarized difference transients for a 4 nm diameter PbS NC sample. The VHVH time base is multiplied by 2 according to eq 1.

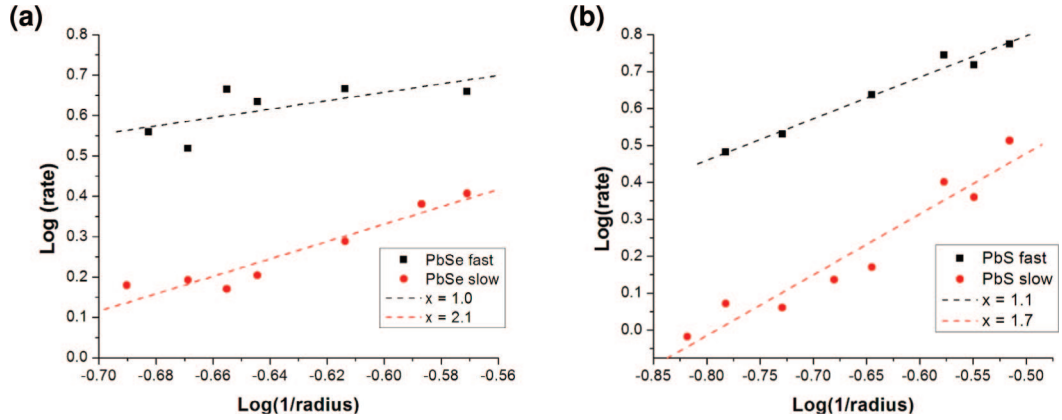

Figure 3. Slow and fast component of biexponential fit for (a) PbSe and (b) PbS. Value of x is based upon fit to $1/r^x$ size dependence of energy splitting on the CPTG decay rate.

able range of our instrument. The free induction decay signal in pure hexane was measured to be typically 5–10 times weaker than the response of the NCs, with no structure outside of pulse overlap. This signal was used as the instrument response for subsequent recovery of the fine structure relaxation time from the convoluted CPTG signals. It should be noted that not all solvents produce an instantaneous free-induction decay signal. Tetrachloroethylene (TCE), a typical solvent with good IR transmission, produces a strong nonresonant signal with a ps oscillatory decay time, probably due to contributions from an optical Kerr effect.

The raw decay signals for VVVV (population grating) and VHVH (spin grating) polarization conditions are displayed in Figure 2 for some of the PbS NC samples. The VVVV signal does not decay considerably on the CPTG time scale because exciton lifetimes are typically $\sim$1 μs for these NCs. After accounting for the instrument response, the decay of VHVH is multiexponential; a satisfactory fit requires either two or three components. The decay constant of the fastest relaxation component was typically similar to or less than the pulse width of the laser, thus its value is not known with high accuracy. This component scales with NC size, but any true size dependence is obscured by the increasing instrument response time as the probe wavelength increases. This component could contain contributions from fast solvent relaxation processes in addition to fine structure relaxation, so it is more difficult to analyze quantitatively than the other two components. This very fast component will be discussed further with regard to its temperature dependence.

Fits for all PbS and PbSe NC sizes are optimized with two exponential decay components (in addition to the very fast component). These two components will be referred to as "fast" and "slow" from here on. The rate constants for both components clearly increase with decreasing size of the NC, as is evident in Figure 2a. For both PbS and PbSe NCs, the fast and slow components have a different dependence on size, with the slow component exhibiting the larger size scaling. The rates of these components vs size are plotted in Figure 3. The trend of the fast component is approximately $1/r$, with the slower component exhibiting a $1/r^2$ dependence. Because of the different size dependences, in the small size regime (d < 4 nm), the rates of the two components become similar (within a factor of 2), making it more difficult to define unique rate constants, thus leading to a larger uncertainty in this range.

Similar fine structure dynamical information to that demonstrated for the CPTG experiment can be obtained from utilizing circularly polarized pump and probe beams in a

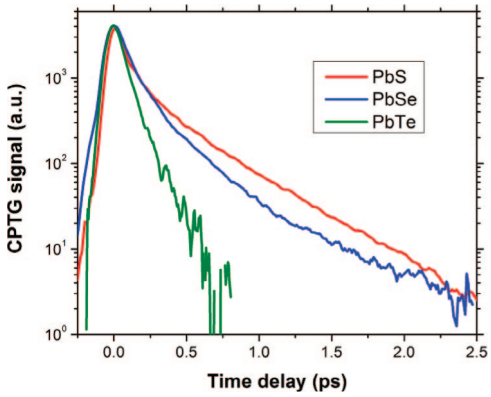

Figure 4. Kinetics of fine structure relaxation for similar sizes (roughly 5 nm diameter) of PbX NCs (X = S, Se, Te).

transient bleaching (TB) experiment. Data for one PbSe NC sample utilizing CPTG and TB experiments are compared in Figure 2b. For pump–probe experiments, the quantity of interest is the RRRR−RRLL signal, which gives the fine structure relaxation rate.[2] Because the signal in a pump–probe configuration is heterodyned, the observed decay rate is governed by:

$$I_{\mathrm{HET}}(t_{\mathrm{pr}}) \propto \int_0^{\infty} \mathrm{Re}\{E^*_{\mathrm{pr}}(t_{\mathrm{pr}})P^{(3)}(0, t_{\mathrm{pr}}, t)\}\mathrm{d}t \qquad (1)$$

Here, $P^{(3)}(t)$ takes the form $\exp[-kt]$, and thus the decay term in homodyne detection (proportional to $P^{(3)}(t)^2$) is $\exp[-2kt]$.

TB traces have lower signal-to-noise ratios than the CPTG results by at least 1 order of magnitude for similar signal integration periods. This is at least partially due to the background-free nature of the CPTG experiment, which allows for the most sensitive and lowest noise detection schemes to be used. Although increasing the pump intensity could improve the TB signal, this may also increase the likelihood that multiexciton effects would influence the spin-flip relaxation dynamics. Although these results would suggest that the TB experiment is less useful for low scattering samples, it may in fact be preferred for samples with poorer optical properties (such as rough films or glasses) because the signal is considerably less sensitive to stray scattered radiation.

The spin-flip relaxation times of PbTe NCs were also measured and compared with results for PbS and PbSe in Figure 4. The measurements reveal much faster rates of fine structure relaxation for these NCs at all sizes. The size dependence of this rate is weak ($x < 1$). In addition to the faster measured rates, it was also noted that the resonant CPTG signal is nearly an order of magnitude weaker in PbTe compared with PbSe and PbS, which have similar signal strengths. It is possible that this weaker observed signal is partially due to the presence of additional fast decay components that are convoluted with the instrument response. Simulations of the CPTG signal under experimental conditions including a fast ($t < 50$ fs) decay component confirms that this leads to a lower observed peak signal. Other mechanisms could also contribute to this lower signal, and these are under further investigation. A summary of the results for one size of all three materials is shown in Table 1.

Table 1. Fit Parameters for CPTG Decay of Three NC Samples

	τ_1 (fs)	τ_2 (fs)	A_2/A_1
PbS	290	790	0.43
PbSe	210	860	0.30
PbTe	145		

The temperature dependence of fine structure relaxation dynamics in 3 nm PbSe NCs is shown in Figure 5. The average decay rate is defined as $k_{\mathrm{ave}} = (A_1k_1 + A_2k_2)/(A_1 + A_2)$, and this quantity is plotted versus temperature. With the value of k_1 and k_2 separated only by a factor of about two, distinct values for all parameters were not always attainable. However, the average decay rate was invariant to fitting procedure and small changes in signal/noise ratio; therefore it is assumed to be an accurate measure of the CPTG decay trend versus temperature. There is a clear trend in both k_{ave} and the amplitude of the CPTG signal A_{peak}. A_{peak} increases as temperature decreases, whereas k_{ave} decreases as the temperature is lowered. These trends are likely the result of the sensitivity of the fine structure relaxation processes to the presence of lattice phonons. One or more optical phonons may be needed to activate transitions between fine structure states. A variety of types and energies of phonons are present at higher temperatures, leading to very fast rates (<50 fs) that contribute to the instrument response limited initial CPTG signal. At lower temperatures, these phonons are not available and this may limit the rate of transitions, especially in the case of a large activation barrier, leading to the ability to measure a rate for this component (k_3, ~80 fs at 12 K) that is longer than the instrument response.

In addition to observing k_3 directly at low temperature, we also detect the influence of k_3 on the observed CPTG peak amplitude (Figure 5a). Because of the finite three pulse cross-correlation time (about 50 fs fwhm), sub-100 fs decay components result in lower measured peak CPTG amplitudes. Although an accurate value of k_3 cannot be determined for all temperatures, the influence of this component can be determined by simulating the convolution of the instrument response with CPTG decays including known values of $k_1(T)$, $k_2(T)$, and expected values of $k_3(T)$. The amplitudes A_x are given by $k_x/(k_1 + k_2 + k_3)$, assuming that the fine structure relaxation can be described by a kinetic scheme in which there are three parallel decay pathways. This is undoubtedly an oversimplification, but it serves the purpose of understanding the temperature dependence.

The temperature dependence of the rate is expected to be proportional to a Boltzmann population factor like $\exp(-E_a/k_BT)$, where E_a is the activation energy of the transition that gives rise to the observed decay. E_a can be fulfilled by one or more optical or acoustic phonons. For the transition associated with k_3, it is expected that the LO phonon is necessary to provide E_a. For k_1 and k_2, a distribution of acoustic phonons may be responsible for mediating the respective transitions. This is also confirmed by the fact that at least two E_a values are necessary to describe the temperature dependence of k_{ave} shown in Figure 5a: one with an energy around 3 meV (transverse optical phonon or sphe-

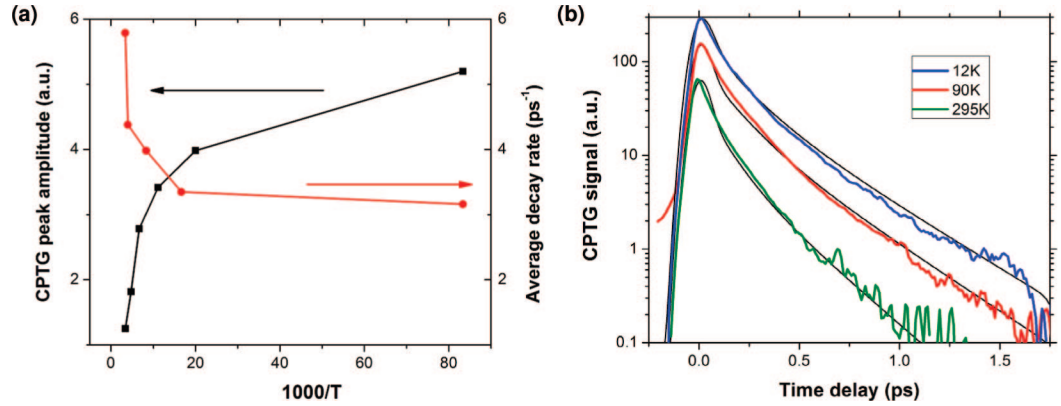

Figure 5. (a) Temperature dependence of CPTG rates and signal amplitudes for 3 nm diameter PbSe NCs in HMN. Lines connecting points are guides to the eye. (b) Simulated signals (black lines) compared with CPTG data (color) for 3 temperatures. k_1 and k_2 values at each temperature are from measured data while the temperature dependence of k_3 is varied to produce agreement with experiment.

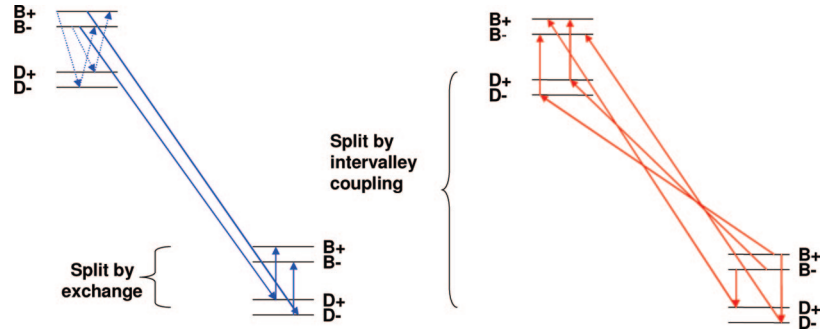

Figure 6. Effective kinetic scheme for a subset of PbX fine structure levels split by two dominant mechanisms. Exciton spin flips can result from sequentially connecting bright (B) and dark (D) states separated by an effective electron (hole) flip. Weakly (blue) and strongly (red) activated transitions can result.

roidal acoustic phonon) and one with an energy ≪1 meV (bath of other acoustic phonons). The temperature dependence of k_3 predicted by simulating the CPTG amplitude suggests that the dominant E_a value for this transition is larger than E_a for k_1 and k_2 by a factor of about 5, implying the influence of LO phonons with an energy near 15 meV. An effective kinetic scheme is shown in Figure 6, which demonstrates the activated nature of some transitions.

Discussion. Considering the number of possible transition pathways with 64 accessible states in PbX NC exciton fine structure, it may be surprising that the spin-flip relaxation signals consist of decays that are primarily biexponential with well-defined rate constants. Moreover, the CPTG signals lack long-lived components that would arise from contributions from states possessing real transition moments (no imaginary part), such as the $F = 0$ state in CdSe.[22] Although these states can be populated during the excitation pulse, they do not result in optical orientation upon interaction with the cross-polarized pump beams, and relaxation to other fine structure states (including those with complex transition moments) does not lead to decay of the CPTG signal because the rotational averaging factor does not change sign during this process.[2] Instead, these states contribute to the TG signal with kinetics that follow population relaxation and an amplitude that is proportional to their oscillator strength. In CdSe nanorods, the long-time offset associated with population of the $F = 0$ state grows with increasing aspect ratio.[6] Determining whether this effect could also occur in PbX requires currently unavailable high-quality shape-controlled PbX samples and additional theoretical detail concerning the transition moments of exciton states as a function of NC shape.

Table 2. Selected Bulk Material Properties of PbX and CdSe From Refs 26, 27

material	ϵ_∞	R_{ex} (nm)	E_g (eV)	SOC (Ry)[a]	m_e	m_h	m_{eff} anisotropy
PbS	17	23	0.40	0.007	0.08	0.075	1.5
PbSe	23	66	0.28	0.031	0.04	0.034	2.0
PbTe	33	152	0.30	0.062	0.024	0.022	12
CdSe	6	5	1.75		0.12	0.80	

[a] Atomic spin–orbit splitting for anion, as in ref 28.

For the spherical NCs we have studied, there are several effects most likely responsible for splitting the exciton fine structure states and affecting the CPTG dynamics: intervalley scattering (IVS), effective mass anisotropy (EMA), electron–hole exchange interactions (EI), and spin–orbit coupling (SOC). The EMA is largest in PbTe (Table 2), which has been discussed previously as a source of broadened exciton features in NCs. This increased energy splitting between fine structure states could give rise to the much larger CPTG decay rates observed in PbTe.[14,24,25] Moreover, because of the presence of the heavy anion Te, PbTe has larger SOC than PbS or PbSe. SOC mixes exciton states with bright and dark character within the lowest absorption manifold, thus inducing transitions between these states. A larger SOC facilitates faster interconversion of states with opposite

angular momentum, leading to a faster CPTG decay rate.

The energy splitting between the bright states of opposite angular momentum projection in the exciton manifold not including IVS has not been explicitly calculated for PbX NCs. However, an estimate of this value in CdSe NCs suggests that this splitting will be very small, not larger than 100 μeV.[29] If this is also true for PbX, the direct transition rates between these states are likely to be much too slow to account for the kinetics we observe. Therefore, it may be that the transitions responsible for the fast decay components arise from opposite angular momentum projection states in separate L valleys split by IVS, with an energy gap predicted to be 10–80 meV.[21] The slower rate could then correspond to either an electron or hole flip between dark and bright exciton states split by EI, with an energy gap of a few meV. Our experimental observation of a larger size dependence for the slow component than for the fast component is consistent with what was determined from the calculations (albeit for only two sizes of PbSe NCs). The assignment of the fast component to IVS-related splitting is also consistent with the larger magnitude of the calculated splitting compared with EI. We are working to determine the transition moments of the various exciton fine structure states which would allow us to constrain a kinetic model (initially involving 64 fine structure states) that could be fit to our data. Including temperature and material dependent signals, this fit should give us more definitive information about the possible origins of the fine structure splitting that give rise to the fast and slow decay pathways.

It was initially suggested by Kim et al.[6] that a fast hole flip is responsible for the dominant fine structure relaxation pathway in CdSe. It was subsequently discovered that a slow component of the CPTG rate also exists for CdSe NCs,[30] although this component does not depend strongly on NC size. This component is suggested to be either due to a direct exciton spin-flip or an electron spin-flip, which would be much slower than the hole spin-flip in CdSe because of the smaller electron effective mass. In PbSe, the effective masses of electrons and holes are similar and lowest conduction and valence band wave functions arise from similar atomic origins, and although it is anticipated that the valence and conduction bands may not have complete mirror symmetry through the energy spectrum,[31] this is still likely to be the case for the lowest exciton band. In that case, we do not expect to resolve separate transitions between states that correspond to electron or hole spin flips because they would have nearly the same rates.

Another difference between CdSe and PbX CPTG signals is that both components of the CPTG decays for PbSe depend on size. In PbS and PbSe, we also observe that the amplitude ratio A_2/A_1 changes as a function of NC size. This ratio increases as the NC size decreases, and as the ratio approaches unity, it becomes more difficult to clearly identify two rates in the observed kinetics. This result suggests that there are two independent and parallel fine structure relaxation pathways that dominate the signal decay. For PbTe, only one rate is identified; however, it is possible that two or more distinct pathways also exist but that the others are faster than the instrument response and cannot be directly measured. As discussed earlier, components much faster than the instrument response could be responsible for reducing the observed resonant signal peak.

If the fast CdSe CPTG component and the slow PbSe CPTG component both involve EI split and SOC-mediated transitions, the question remains why the dependences of the CPTG decay rate on size are so different ($x = 4$ for CdSe, $x = 2$ for PbX). We offer several possible sources of this much weaker size dependence of fine structure splitting in PbX: (1) finite potential barrier effects, much more pronounced in PbX because of the very small hole and electron effective masses, mitigate the expected size dependence from simple effective-mass models; (2) long-range EI may arise from monopole-like contributions from separate unit cells in PbX,[32] leading to a energy dependence like $1/r$ (and thus $1/r^2$ in the rate); (3) dielectric screening effects, much larger in PbX than in CdSe, could reduce Coulomb-like energy splitting. We are not yet in a position to definitively discern between these and other effects. However, further theoretical work and continued CPTG experiments in other nanocrystalline materials should provide new insight.

Conclusions. In advance of future theoretical work, which is necessary to rigorously model the fine structure relaxation in PbX NCs, we offer several important qualitative conclusions that can be drawn from the CPTG experiments. There are two dominant resolvable fine structure relaxation pathways for PbS and PbSe and one that involves rates much faster than our instrument resolution. The slowest rates are consistent with transitions between states split by electron–hole exchange interactions while the fastest rates are more likely between states arising from L valley splitting. The fine structure relaxation pathways occur in parallel, with each having a unique dependence on size. The intrinsic size dependence is most likely dictated by the electronic matrix element for each transition predicted by theory and not due solely to electron–phonon coupling size dependences, although coupling to phonons plays a role in the activation of some fine structure transitions. In addition, we find that all accessible bright fine structure states must have complex transition moments, and the size dependence of the fine structure splitting is greatly overestimated by conventional effective-mass approximation considerations. Finally, the CPTG rates are the fastest in PbTe, likely due to spin–orbit coupling and/or effective mass anisotropy effects. These conclusions may guide future theoretical efforts to produce more detailed identification of these fine structure states and the coupling between them.

Acknowledgment. We thank Evident Technologies for providing PbS samples. We are indebted to Alberto Franceschetti and Jeongho Kim for insightful discussions. K.A.G. acknowledges the support of an NSF-IGERT fellowship. This work was supported by the U.S. Department of Energy, Office of Basic Energy Sciences, Division of Chemical Sciences, Biosciences, and Geosciences. This work was supported by the U.S. Department of Energy under contract no. DE-AC36-99GO10337 with the National Renewable Energy Laboratory.

References

(1) (a) Zutic, I.; Fabian, J.; Das Sarma, S. *Rev. Mod. Phys.* **2004**, *76*, 232. (b) *Semiconductor Spintronic and Quantum Computation*; Awschalom, D. D., Loss, D., Samarth, N., Eds.; Springer: Berlin, 2002.
(2) Scholes, G. D. *J. Chem. Phys.* **2004**, *121*, 10104.
(3) Huxter, V. M.; Kovalevskij, V.; Scholes, G. D. *J. Phys. Chem. B* **2005**, *109*, 20060–20063.
(4) Scholes, G. D.; Kim, J.; Wong, C. Y.; Huxter, V. M.; Nair, P. S.; Fritz, K. P.; Kumar, S. *Nano Lett.* **2006**, *6*, 1765–1771.
(5) Scholes, G. D.; Kim, J.; Wong, C. Y. *Phys. Rev. B* **2006**, *73*, 195325.
(6) Kim, J.; Wong, C. Y.; Nair, P. S.; Fritz, K. P.; Kumar, S.; Scholes, G. D. *J. Phys. Chem. B* **2006**, *110*, 25371–25382.
(7) Furis, M. A.; Htoon, H.; Petruska, M.; Klimov, V. I.; Barrick, T.; Crooker, S. A. *Phys. Rev. B* **2006**, *7*, 3–241313.
(8) Kang, I.; Wise, F. W. *J. Opt. Soc. Am. B* **1997**, *14*, 1682.
(9) Wei, S.; Zunger, A. *Phys. Rev. B* **1997**, *55*, 13605.
(10) Wise, F. W. *Acc. Chem. Res.* **2000**, *33*, 773.
(11) Allan, G.; Delerue, D. *Phys. Rev. B* **2004**, *70*, 245321.
(12) Schaller, R. D.; Klimov, V. I. *Phys. Rev. Lett.* **2004**, *92*, 186601.
(13) Ellingson, R. J.; Beard, M. C.; Johnson, J. C.; Yu, P. R.; Micic, O. I.; Nozik, A. J.; Shabaev, A.; Efros, A. L. *Nano Lett.* **2005**, *5*, 865.
(14) Murphy, J. E.; Beard, M. C.; Norman, A. G.; Ahrenkiel, S. P.; Johnson, J. C.; Yu, P. R.; Micic, O. I.; Ellingson, R. J.; Nozik, A. J. *J. Am. Chem. Soc.* **2006**, *128*, 3241–3247.
(15) Shabaev, A.; Efros, A. I.; Nozik, A. J. *Nano Lett.* **2006**, *6*, 2856.
(16) Fleming, G. R.; Cho, M. *Annu. Rev. Phys. Chem.* **1996**, *47*, 109.
(17) de Boeij, W. P.; Pshenichnikov, M. S.; Wiersma, D. A. *Annu. Rev. Phys. Chem.* **1998**, *49*, 99.
(18) Fourkas, J. T.; Trebino, R.; Fayer, M. D. *J. Chem. Phys.* **1992**, *97*, 69.
(19) Franceschetti, A.; Zunger, A. *Phys. Rev. Lett.* **1997**, *78*, 915.
(20) An, J. M.; Franceschetti, A.; Dudiv, S. V.; Zunger, A. *Nano Lett.* **2006**, *6*, 2728.
(21) An, J. M.; Franceschetti, A.; Zunger, A. *Nano Lett.* **2007**, *7*, 2129.
(22) Efros, A. L.; Rosen, M.; Kuno, M.; Nirmal, M.; Norris, D. J.; Bawendi, M. *Phys. Rev. B* **1996**, *54*, 4843.
(23) Hines, M. A.; Scholes, G. D. *Adv. Mater.* **2003**, *15*, 1844.
(24) Tudury, G. E.; Marquezini, M. V.; Ferreira, L. G.; Barbosa, L. C.; Cesar, C. L. *Phys. Rev. B* **2000**, *62*, 7357.
(25) Zhang, Y.; Mascarenhas, A.; Jones, E. D. *J. Appl. Phys.* **1998**, *83*, 448.
(26) Ravich, Y. I.; Lead chalcogenides: basic physical features. In *Lead Chalcogenides: Physics and Applications*; Khokhlov, D., Ed.; Taylor and Francis: New York, 2003.
(27) Laheld, U. E. H.; Einevoll, G. T. *Phys. Rev. B* **1997**, *55*, 5184.
(28) Lin, P. J.; Kleinman, L. *Phys. Rev.* **1965**, *142*, 478.
(29) Franceschetti, A. unpublished results.
(30) Wong, C.; Kim, J.; Scholes, G. D. in preparation.
(31) An, J.; Franceschetti, A.; Dudiy, S. V.; Zunger, A. *Nano Lett.* **2006**, *6*, 2728.
(32) Franceschetti, A.; Wang, L.; Fu, H.; Zunger, A. *Phys. Rev. B* **1998**, *58*, R13367.

NL080126A